**Motoneuron degeneration in the trigeminal motor nucleus innervating the masseter muscle in *dystonia musculorum* mice**

**MD Ibrahim Hossain[a,b], Masao Horie[a], Nozomu Yoshioka[a,c], Masayuki Kurose[d], Kensuke Yamamura[d], Hirohide Takebayashi[a,*]**

[a]Division of Neurobiology and Anatomy, Graduate School of Medical and Dental Sciences, Niigata University, Niigata 951-8510, Japan
[b]Department of Biochemistry and Molecular Biology, Jahangirnagar University, Savar, Dhaka 1342, Bangladesh
[c]Transdisciplinary Research Program, Niigata University, Niigata 951-8510, Japan
[d]Division of Oral Physiology, Niigata University Graduate School of Medical and Dental Sciences, Niigata University, Niigata 951-8514, Japan

Present address of MH
Department of Morphological Sciences, Graduate School of Medical and Dental Sciences, Kagoshima University, Kagoshima 890-8544, Japan

*Corresponding author. Division of Neurobiology and Anatomy, Graduate School of Medical and Dental Sciences, Niigata University, Niigata 951-8510, Japan.
E-mail: takebaya@med.niigata-u.ac.jp (H. Takebayashi)

*Abbreviations used:* ATF3, activating transcription factor 3; AUC, area under the curve; BP230, the 230kDa bullous pemphigoid antigen; BPAG1, bullous pemphigoid antigen 1; CNS, central nervous system; ChAT, choline acetyltransferase; CHOP, C/EBP homologous protein; CTB, cholera toxin B subunit; DAPI, 4′,6-diamidino-2-phenylindole; DRG, dorsal root ganglia; *Dst*, *Dystonin*; EMG, electromyography; GFAP, glial fibrillary acidic protein; HE, hematoxylin and eosin; HSAN6, hereditary sensory autonomic neuropathy type VI; IHC, immunohistochemistry; ISH, *in situ* hybridization; KO, knockout; Lcn2, lipocalin 2; MBP, myelin basic protein; Mo5, trigeminal motor nucleus; NF, neurofilament; PFA, paraformaldehyde; P, postnatal days; PNS, peripheral nervous system; V3, mandibular nerve.

**Abstract**

*Dystonia musculorum* (*dt*) mice, which have a mutation in the *Dystonin* (*Dst*) gene, are used as animal models to investigate the human disease known as hereditary sensory and autonomic neuropathy type VI. Massive neuronal cell death is observed, mainly in the peripheral nervous system (PNS) of *dt* mice. We and others have recently reported a histopathological feature of these mice that neurofilament (NF) accumulates in various areas of the central nervous system (CNS), including motor pathways. Although *dt* mice show motor disorder and growth retardation, the causes for these are still unknown. Here we performed histopathological analyses on motor units of the trigeminal motor nucleus (Mo5 nucleus), because they are a good system to understand neuronal responses in the mutant CNS, and abnormalities in this system may lead to problems in mastication, with subsequent growth retardation. We report that motoneurons with NF accumulation in the Mo5 nuclei of $Dst^{Gt}$ homozygous mice express the stress-induced genes *CHOP*, *ATF3*, and *lipocalin 2 (Lcn2)*. We also show a reduced number of Mo5 motoneurons and a reduced size of Mo5 nuclei in $Dst^{Gt}$ homozygous mice, possibly due to apoptosis, given the presence of cleaved caspase 3-positive Mo5 motoneurons. In the mandibular (V3) branches of the trigeminal nerve, which contains axons of Mo5 motoneurons and trigeminal sensory neurons, there was infiltration of Iba1-positive macrophages. Finally, we report atrophy of the masseter muscles in $Dst^{Gt}$ homozygous mice, which showed abnormal nuclear localization of myofibrils and increased expression of *atrogin-1* mRNA, a muscle atrophy-related gene and weaker masseter muscle strength with uncontrolled muscle activity by electromyography (EMG). Taken together, our findings strongly suggest that mastication in *dt* mice is affected due to abnormalities of Mo5 motoneurons and masseter muscles, leading to growth retardation at the post-weaning stages.

*Keywords*: *dystonia musculorum*; trigeminal motor nucleus (Mo5); motor neuron; neurodegeneration; mandibular nerve; masseter muscle.

## 1. Introduction

*Dystonia musculorum* (*dt*) mice were originally characterized as a naturally occurring spontaneous mouse mutant, showing motor disorder, dystonia and cerebellar ataxia, as well as sensory neuron degeneration in the early postnatal period (Duchen et al., 1963; Duchen et al., 1964). Mutation of the *Dystonin* (*Dst*) gene, encoding Dystonin, a cytoskeletal linker protein, causes *dt* phenotypes (Brown et al., 1995; Guo et al., 1995). It has also been reported that loss-of-function mutations in the human *DST* gene cause hereditary sensory and autonomic neuropathy type VI (HSAN6) (Edvardson et al., 2012; Manganelli et al. 2017), and/or epidermolysis bullosa simplex (EBS), a skin blistering disease (Groves et al. 2010). Appearance of manifestation depends on affected isoform(s) by the mutation, neural isoform and/or skin isoform. HSAN6 is characterized by progressive sensory neuropathy and a varying degree of autonomic dysfunction. Since some HSAN6 patients and *dt* mice have a similar phenotype, with decreased longevity and a mutation in the same gene, *dt* mice are good mouse models for understanding HSAN6 pathogenesis.

There are three main isoforms of *Dst* (*Dystonin-a*, *Dystonin-b*, and *Dystonin-e*), which are predominantly expressed in the nervous system, muscles, and skin, respectively (Leung et al., 2001; Young and Kothary, 2007). Dystonin-e protein was initially identified as BPAG1, also known as BP230, one of the major autoantigens in the skin blistering disease, bullous pemphigoid (Westgate et al., 1985). Among the three isoforms, *Dystonin-a* is predominantly expressed in the nervous system, and encodes a very large protein (615 kDa in mouse) containing various domains, including some which interact with the cytoskeleton, such as an actin-binding domain and a tubulin binding domain (Leung et al., 1999; Leung et al., 2001;

Okumura et al., 2002; Young and Kothary, 2007). It has been suggested that loss of the *Dystonin-a2* isoform accounts for part of the *dt* phenotype (Ferrier et al., 2014; Manganelli et al., 2017; Ryan et al., 2012a; 2012b).

In addition to the sensory degeneration originally identified in the dorsal root ganglia (DRG) of *dt* mice, histological abnormalities in the motor pathway of *dt* mice have recently been described. Abnormal accumulation of neurofilament (NF), a neuronal intermediate filament protein, was reported in the sensory neurons in the DRG (Janota, 1972), in a subset of neurons in the spinal cord (Campbell and Peterson, 1992; Dowling et al., 1997), and later, in motor-related nuclei in the brainstem (Horie et al., 2016; Seehusen et al., 2016). Abnormal cellular translocation of α-internexin, another neuronal intermediate filament protein, has also been reported in the spinal motor neurons of *dt* mice (Tseng et al., 2008). Gradual progress has been made on understanding of CNS abnormalities in *dt* mice, and a reduced number of neurons has been reported in the trigeminal motor nucleus (Mo5), and spinal cord motoneurons at the lumber level (De Repentigny et al., 2011; Horie et al., 2014).

In the present study, we performed detailed histopathological and electrophysiological analyses on Mo5 motoneurons and their target muscle, the masseter muscle, in $Dst^{Gt}$ homozygotes. These are important motor units for mastication (Li et al., 1995), abnormalities in which may therefore influence the systemic condition of *dt* mutants (N'gom et al., 2002). Here, we report the degeneration of $Dst^{Gt}$ homozygous Mo5 motoneurons, characterized by various abnormalities including induction of CHOP (an endoplasmic reticulum stress marker; Wolfgang et al., 1997), ATF3 (a stress marker; Hai et al., 1999), Lcn2 (a stress marker; El Karoui et al., 2015), and cleavage of caspase 3 (an apoptotic marker). We also observed infiltration of macrophages in the mandibular (V3) branches of the trigeminal nerve, and atrophy of the masseter muscle in the $Dst^{Gt}$ homozygous mice.

## 2. Materials and Methods

### 2.1 Mice

The *Dst* gene trap mutant mice (*Dst*$^{Gt}$ mice; Horie et al., 2014) were backcrossed to C57BL/6NCrj mice (Charles River Japan Inc., Kanagawa, Japan) for at least six generations. The day of birth was considered to be postnatal day zero (P0). Since *Dst*$^{Gt}$ homozygous mice start to die before 4 weeks of age, postnatal day 28 (P28) is considered as the late stage of the *dt* phenotype. In order to increase longevity, we manually gave food paste to *Dst*$^{Gt}$ homozygous mice twice a day. We also gave them *ad libitum* access to food paste. All procedures were approved by the animal research committee at Niigata University. The National Institutes of Health guide for the care and use of laboratory animals was followed.

### 2.2 Genotyping

The *Dst*$^{Gt}$ mice were genotyped by polymerase chain reaction using extracted genomic DNA, as previously described (Horie et al., 2014).

### 2.3 Neuronal tracing

Neuronal tracing experiments were performed as previously reported (Horie et al., 2013). Glass capillary pipets were made from micro-capillaries (Microcap 50 μl, 1-000-0500, Drummond Scientific Co., Broomall, PA, USA) using a horizontal-type puller (PC-10, Narishige, Tokyo, Japan). Four C57BL/6N control mice and four *Dst*$^{Gt}$ homozygous mice, at 18 days old (P18), were used for neuronal tracing. Animals were anesthetized with an intraperitoneal injection (3 ml/kg body weight) of a mixture of ketamine (80 mg/ml, Ketalar; Daiichi-Sankyo, Tokyo, Japan) and xylazine (10 mg/ml; Selactar; Bayer Medical Ltd., Tokyo, Japan). After the left masseter muscle was exposed, a glass capillary pipet (tip inside diameter: 20–30 μm), filled with 0.5% cholera toxin B subunit (CTB, List Biological

Laboratories, Campbell, CA, USA), was inserted into the muscle, and 0.1 μl of CTB was injected. To prevent backflow, the glass capillary was maintained in place for 30 sec after the completion of the pressure injection. Three days later, mice were sacrificed for histological experiments.

2.4 Hematoxylin and eosin (HE) staining and immunohistochemistry (IHC)

To make paraffin sections, mice were anesthetized with an intraperitoneal injection of a lethal dose of sodium pentobarbital (125 mg/kg body weight) and then perfused transcardially with approximately 2 mL of 0.01M phosphate-buffered saline, followed by 20–25 mL of 0.1M phosphate buffer containing 4% paraformaldehyde (PFA). Brains and spinal cords were removed and immersed in 4% PFA overnight, and then embedded in paraffin. Consecutive 10 μm thick coronal sections were cut using a rotary microtome (HM 325; MICROM; RM2245, Leica Microsystems, Wetzlar, Germany).

HE staining was performed as previously described (Takebayashi et al., 2002). IHC was performed as previously described (Horie et al., 2014; Takebayashi et al., 2002), using the following antibodies and dilutions: mouse monoclonal anti-NF-M (1C8; 1:15) (Horie et al., 2016; Watanabe et al., 2006), rabbit polyclonal anti-glial fibrillary acidic protein (GFAP) (Z0334, 1:1,000, DAKO, Glostrup, Denmark), mouse monoclonal anti-myelin basic protein (MBP) (QD-9, 1:100, Abcam, Cambridge, UK), rabbit polyclonal anti-Iba1 (WAKO, 1:500), rabbit polyclonal ATF3 (1:300, Santa Cruz Biotechnology, Santa Cruz, CA, USA), rabbit monoclonal anti-cleaved caspase 3 (#9664, 1:500, Cell Signaling Technology, Danvers, MA, USA), goat polyclonal anti-choline acetyltransferase (ChAT) (AB144P, 1:200, Merck Millipore, Billerica, MA, USA), goat polyclonal anti-lipocalin 2 (Lcn2) (1:100, R&D systems, Minneapolis, MN, USA), goat polyclonal anti-CTB (#703, 1:40,000, List Biological Laboratories, Campbell, CA, USA), mouse monoclonal anti-MYH6 (clone S46, 1:20,

Developmental Studies Hybridoma Bank, Iowa City, IA, USA), peroxidase-labeled anti-mouse, anti-rabbit IgG, and anti-goat IgG antibodies (1:200, Medical and Biological Laboratories, Nagoya, Japan), Alexa Fluor 488-labeled goat anti-mouse IgG, and Alexa Fluor 594-labeled goat anti-rabbit IgG antibodies (1:1,000, Invitrogen/ThermoFisher Scientific Inc., Waltham, MA, USA).

2.5 *In situ* hybridization (ISH)

ISH was performed on paraffin sections as previously described (Horie et al., 2014). The following mouse ISH probes were used: *CHOP* (also known as *DNA-damage inducible transcript 3* (*Ddit3),* or *gadd153*; Ikeda et al., 2017), *activating transcription factor 3* (*Atf3*, Genbank accession number: BC064799), *choline acetyltransferase* (*ChAT*, Furusho et al., 2006), *lipocalin 2* (*Lcn2*, also known as *24p3*, or *NGAL*; Genbank accession number: NM_008491), and *atrogin-1* (also known as *F-box protein 32* (*Fbxo32*), Genbank accession number: NM_026346, nt 435-1085).

Transmitted light images and fluorescent images were taken with an Olympus BX53 microscope connected to a CCD camera (DP72 or DP74; Olympus, Tokyo, Japan).

2.6 Quantification analyses

For the quantification of NF-, *CHOP*-, *ATF3*- and *Lcn2*-positive cells on transverse sections of brain stem at P21 and P28, four wild-type mice and four $Dst^{Gt}$ homozygous mice were used. After staining with anti-NF antibody or specific probes, positive cells in the Mo5 nuclei were manually counted in the both Mo5 nucleus in the section. Results were represented as number of positive Mo5 motoneurons per section.

In order to count the total number of Mo5 motoneurons and to measure the size of Mo5 nuclei, three wild-type mice and three $Dst^{Gt}$ homozygous mice at P28 were used. After

perfusion and paraffin embedding, coronal sections of the brainstem were cut serially at 10 μm thickness, and then the sections were placed on serially numbered glass slides starting just before the Mo5 nucleus, as confirmed by Nissl staining. Five slides were used to collect all the serial sections containing the Mo5 nucleus. After staining with anti-ChAT antibody, we manually counted all the ChAT-positive neurons in each Mo5 nucleus. To measure the size of Mo5 nuclei, we counted the number of sections, which contained ChAT-positive Mo5 motoneurons. Then, the size of Mo5 nuclei (diameter along the rostro-caudal axis) was calculated as follows: (total number of sections containing Mo5) ×10 μm.

For the quantification of the number of nuclei in the V3 nerve, we performed HE staining on the sections of three wild-type mice and three *Dst*$^{Gt}$ homozygous mice at P28, and then, took pictures using BX53 microscope connected to a CCD camera (DP72 or DP74; Olympus, Tokyo, Japan). The numbers of nuclei were manually counted in the randomly selected area from each V3 nerve section (approximately 5000 μm$^2$/section). Results were represented as number of nuclei per mm$^2$ area.

2.7 Electromyography (EMG)

The animals (four *Dst*$^{Gt}$ homozygous mice at P24-P26 and three control mice at P24) were anesthetized with 2–3% isoflurane (Pfizer, Tokyo, Japan: RM-600; Aika Medical). Two percent lidocaine (Xylocaine; Dentsply, Tokyo, Japan) was injected into the skin to minimize surgical pain before the incisions were made. Depth of anesthesia was checked repeatedly throughout the experiment by pinching the paws. A midline incision was made along the ventral aspect of the mandible. Paired copper wire electrodes with an exposed tip were implanted into right side of masseter as a jaw-closing muscle and the suprahyoid as a jaw-opening muscle to record electromyographic activities. Signals from both muscles were amplified using AC amplifiers (band pass: 0.1–3 kHz), and the signals were fed into a

computer equipped with CED Power 1401 board and analysis software (Spike2; Cambridge Electronic Design Ltd., Cambridge, UK). The sampling rate for the EMGs was 2000/s. After recovery from anesthesia, recordings were carried out at both resting state and active eating state. For active-state EMG recording, animals were fed test food, a standardized amount of cheese in a cube shape (2 mm x 2 mm x 2mm). The data were obtained from stable chewing cycles (five continuous cycles). Measured parameters were mean duration and amplitude (i.e. area under the curve (AUC)) of each masseter muscle bursts (Ariyasinghe et al. 2004; Ootaki et al., 2004).

### 2.8 Statistics

Data, which followed a Gaussian distribution, were analyzed by *t-test* (number of Mo5 motoneurons, size of Mo5 nucleus, number of nuclei in the V3 nerve and EMG data). Other data (NF accumulation, *CHOP*-, *ATF3*- *Lcn2*-, cleaved caspase 3-positive cells) were analyzed by Mann-Whitney U test. Statistical analysis was conducted using SPSS Statistics software, version 22 (IBM, Armonk, NY). Results are represented as Mean ± SEM. $P < 0.05$ was considered statistically significant.

## 3. Results

### *3.1 Induction of stress markers in neurons with NF accumulation in the Mo5 nuclei of $Dst^{Gt}$ homozygous mice*

NF accumulation in the cytoplasm and axons is the hallmark of abnormal neurons in *dt* mice, both in the PNS and CNS. NF IHC revealed abnormal NF accumulations were also present in neuronal cell bodies and axons (called spheroids) in the Mo5 nuclei of $Dst^{Gt}$ homozygotes at P28 (Fig. 1A, B, D; wild-type: 0 ± 0/section, $Dst^{Gt}$ homozygotes: 3.00 ± 0.29/section, $P < 0.05$), in addition to previously reported nuclei in the CNS, such as lateral

vestibular nucleus, reticular nucleus and red nucleus (Horie et al., 2016; Seehusen et al., 2016). In order to examine the state of cellular stress, we performed ISH for *CHOP* and *ATF3*. We found that *CHOP*-positive and *ATF3*-positive cells were present in the $Dst^{Gt}$ homozygous Mo5 nuclei, but not in the wild-type Mo5 nuclei at P28 (Fig. 1B, E, F; *CHOP*, wild-type: 0 ± 0 cells/section, $Dst^{Gt}$ homozygotes: 2.30 ± 0.71 cells/section, $P < 0.01$; *ATF3*, wild-type: 0 ± 0 cells/section, $Dst^{Gt}$ homozygotes: 5.13 ± 0.24 cells/section, $P < 0.05$). NF accumulation, expression of *CHOP* and *ATF3* were also observed in the P21 $Dst^{Gt}$ homozygous Mo5 nuclei (Fig. 1D-F; NF, wild-type: 0 ± 0 cells/section, $Dst^{Gt}$ homozygotes: 2.83 ± 0.33 cells/section, $P < 0.05$; *CHOP*, wild-type: 0.25 ± 0.25 cells/section, $Dst^{Gt}$ homozygotes: 1.50 ± 0.35 cells/section, $P < 0.05$; *ATF3*, wild-type: 0.17 ± 0.16 cells/section, $Dst^{Gt}$ homozygotes: 5.830 ± 1.94 cells/section, $P < 0.05$). To determine whether the expression was co-localized, we performed double staining for NF IHC and *CHOP* ISH, and NF IHC and *ATF3* ISH. Figure 1C shows abnormal NF accumulation is co-localized with *CHOP* signals (Fig. 1C; g, g') and *ATF3* signals (Fig. 1C; h, h'). We also confirmed the co-localization between ATF3 and *CHOP* (Fig. 1C; i, i'), which is consistent with a previous report that CHOP is a target of ATF3 (Wolfgang et al., 1997). These data suggest that neurons in the Mo5 nuclei of $Dst^{Gt}$ homozygotes with abnormal accumulation of NF are in a stressed condition.

### *3.2 Lipocalin 2 expression in Mo5 motoneurons of $Dst^{Gt}$ homozygous mice*

Lipocalin-2 (Lcn2) is an acute phase secreted protein induced in response to various stimuli, such as cellular stress, injury, infection, or inflammation (Jha et al., 2015; El Karoui et al., 2015; Nilsen-Hamilton et al., 2003). Lcn2 is implicated in both pro-apoptotic effects (Chien et al., 2012; Devireddy et al., 2001; Lee et al., 2007; Liu et al., 2011; Tong et al., 2003) and anti-apoptotic effects (Halabian et al., 2013; Tong et al., 2005), depending on the context. It has also been reported that *Lcn2* is a target gene of ER stress pathways (Hsin et al.,

2012; El Karouli et al., 2015). We found increased expression of *Lcn2* mRNA (Fig. 2A, B; wild-type: 0 ± 0 cells/section, $Dst^{Gt}$ homozygotes: 9.17 ± 0.33 cells/section, $P < 0.05$) and Lcn2 protein (Fig. 2A; c, d) in the neurons of $Dst^{Gt}$ homozygous Mo5 nuclei at P28. Expressions of *Lcn2* were also significantly higher in $Dst^{Gt}$ homozygous Mo5 nuclei than wild-type both at P21 (Fig. 2B; wild-type: 0.33 ± 0.33 cells/section, $Dst^{Gt}$ homozygotes: 8.83 ± 0.88 cells/section, $P < 0.05$). To confirm that *Lcn2* expression was actually in the motoneurons innervating masseter muscle, we injected the retrograde neural tracer, CTB, into the masseter, and then detected CTB transported to the soma of Mo5 motoneurons by IHC. Although CTB signals were observed both in the motoneurons of wild-type and $Dst^{Gt}$ homozygous mice at P21 (Fig. 2C; e, f), co-localization with *Lcn2* signals was observed only in the $Dst^{Gt}$ homozygous Mo5 motoneurons (Fig. 2C; h). Taken together, these data suggest that stress in Mo5 motoneurons in $Dst^{Gt}$ homozygotes leads to Lcn2 induction and secretion.

### *3.3 Reduced number of Mo5 motoneurons and reduced size of Mo5 nuclei in $Dst^{Gt}$ homozygous brainstem*

Since we observed induction of stress markers in the motoneurons with NF accumulation in the Mo5 nuclei of $Dst^{Gt}$ homozygote mice at P28, we performed ChAT staining to examine the number of motoneurons and the size of Mo5 nuclei (Fig. S1). ChAT IHC revealed that the number of Mo5 motoneurons in the $Dst^{Gt}$ homozygotes was reduced at P28 (Fig. 3A). Statistical analysis revealed that the reduction in number of Mo5 motoneurons was significant (Fig. 3B; wild-type 2395.72 ± 112.35 neurons/mouse, $Dst^{Gt}$ homozygotes 2053.98 ± 39.87 neurons/mouse, $P < 0.05$). This observation led us to measure the size of the Mo5 nuclei. We found that the diameter along the rostro-caudal axis was also significantly reduced in the brainstem of $Dst^{Gt}$ homozygotes at P28 (Fig. 3C; wild-type 550 ± 14.45 μm/mouse, $Dst^{Gt}$ homozygotes 441.67 ± 16.68 μm/mouse, $P < 0.01$). These data strongly

suggest that stressed Mo5 motoneurons degenerated during *dt* pathogenesis, which ultimately resulted in a reduced size of Mo5 nuclei in the $Dst^{Gt}$ homozygotes.

### *3.4 Apoptosis of Mo5 motoneurons in the $Dst^{Gt}$ homozygous mice*

In order to provide evidence for cell death of Mo5 motoneurons in the $Dst^{Gt}$ homozygotes, we performed IHC using a sensitive rabbit monoclonal anti-cleaved caspase 3 antibody. As expected, we found cleaved caspase 3-positive neurons in the Mo5 nuclei of $Dst^{Gt}$ homozygotes at P28 (Fig. 4B; b). Statistical analysis also showed that the increased number of cleaved caspase 3-positive cells in the Mo5 nuclei was significant (Fig. 4C; wild-type 0.083 ± 0.084/section, $Dst^{Gt}$ homozygotes 3.50 ± 0.288/section, $P < 0.05$). Double staining with *ChAT* ISH and cleaved caspase 3 IHC identified cells double positive for these two markers (Fig. 4B; d, insets), showing that Mo5 motoneurons of $Dst^{Gt}$ homozygous mice are dying at P28. Interestingly, we also observed some cleaved caspase 3 single positive cells, which were not positive for *ChAT* (Fig. 4B; d), in the Mo5 nuclei of $Dst^{Gt}$ homozygotes. Therefore, there is the possibility that some interneurons in the Mo5 nuclei are also dying during the progression of pathology. Finally, we confirmed that neurons with NF accumulation in $Dst^{Gt}$ homozygous Mo5 nuclei were also positive for cleaved caspase 3 (Fig. 4D), using double fluorescent IHC. We also performed cleaved caspase 3 staining at P21 and found positive cells in some $Dst^{Gt}$ homozygous mice, suggesting that onset of caspase 3 activation is around P21 (data not shown). These data indicate that motoneurons with NF accumulation in Mo5 nuclei undergo apoptosis by the activation of caspase 3.

### *3.5 Macrophage infiltration into the V3 nerve in $Dst^{Gt}$ homozygous mice*

Since Mo5 motoneurons control the movement of the masseter muscle, innervating through the mandibular (V3) nerve (Li et al., 1995), and Mo5 motoneurons degenerate in

*Dst*$^{Gt}$ homozygotes, we next examined the histopathology of the V3 nerve. Previously, irregular and disorganized myelin was reported in the *Dst*$^{Gt}$ homozygous trigeminal nerve by MBP IHC, and axon degeneration with myelin breakdown was confirmed by electron microscopic analysis (Horie et al., 2014). HE staining of transverse sections showed significantly higher number of nuclei in the V3 nerve of *Dst*$^{Gt}$ homozygous mice than in wild-type mice (Fig. 5A, B; wild-type 14573 ± 1562.22 nuclei/mm$^2$, *Dst*$^{Gt}$ homozygotes 35515 ± 80.09 nuclei/mm$^2$, $P < 0.01$). We subsequently identified that these additional cells were Iba1-positive macrophages, not GFAP-positive satellite glial cells (Fig. 5C). Since the V3 nerve contains degenerating sensory axons and myelin in *dt* mice (Ichikawa et al., 2008; Horie et al., 2014; Sotelo and Guenet, 1988), it is possible that these macrophages were infiltrating into the V3 nerve in response to sensory neuropathy. Fluorescent double IHC revealed that many Iba1-positive macrophages contacted MBP-positive Schwann cells in the V3 nerve (Fig. 5D; g-l), suggesting that the macrophages were eliminating degenerating myelin.

### *3.6 Atrophy, muscle spindle degeneration and weak muscular activity in the Dst$^{Gt}$ homozygous masseter muscle*

Since we observed reduced numbers of Mo5 motoneurons, we examined their target muscle, the masseter (Baverstock et al., 2013), in *Dst*$^{Gt}$ homozygous mice. Masseter muscles of *Dst*$^{Gt}$ homozygous mice were smaller and thinner than those of wild-type mice at P28 (Fig. 6A). HE staining of the masseter showed increased numbers of nuclei in the *Dst*$^{Gt}$ homozygous mice, indicating degeneration of these muscle fibers (Fig. 6B; a, b). We also confirmed the atrophy of *Dst*$^{Gt}$ homozygous masseter muscle by increased expression of *atrogin-1* mRNA (Fig. 6C), which is a well-known marker for skeletal muscle atrophy (Gomes et al., 2001; Sandri et al., 2004). Since muscle spindle degeneration had been

reported in *dt* mice (Dowling et al., 1997, Duchen et al., 1963), we also examined the muscle spindles of the masseter muscle. HE staining showed that the muscle spindles of wild-type masseter were fine in shape and well-structured (Fig. 6D; g,h), whereas those of $Dst^{Gt}$ homozygous masseter muscle were either swollen (Fig. 6D; i) or degenerated (Fig. 6D; j). We also confirmed the muscle spindle phenotype using MYH6 IHC, which stains the intrafusal fibers of muscle spindles (Fig. 6D; k-n). We also performed EMG recording, in which $Dst^{Gt}$ homozygous mice showed overlap of agonist (jaw-closing)-antagonist (jaw-opening) muscle activities (co-contraction) at resting state, which rarely occurred in the control mice (Fig. 7A). Furthermore, EMG data at active state during cheese-eating suggested weaker contraction in the masseter muscle of the $Dst^{Gt}$ homozygous mice than that in the control mice (Fig. 7B). The notion was supported by smaller amplitude (i.e. AUC) of chewing-related activity of the masseter muscle in the $Dst^{Gt}$ homozygous mice than that in the control mice (Fig. 7D; $*P < 0.05$), despite no significant difference in the duration of the muscle activity between the groups (Fig. 7C) Together, these data suggest that the masseter muscles of *dt* mice have weak and uncoordinated movement, probably due to muscle atrophy and/or neurogenic factor.

## 4. Discussion

In this study, we have shown that there was degeneration of Mo5 motoneurons and a reduction in the size of Mo5 nuclei in $Dst^{Gt}$ homozygous mice and that the neurons with abnormal NF accumulation also expressed the stress markers *CHOP, ATF3*, and *Lcn2*. We also demonstrated macrophage infiltration into the V3 nerve and masseter muscle atrophy with weak muscle contraction. All these data suggest that *dt* mice having difficulty in mastication of food, which may be one of the reasons for growth retardation at the post-weaning stage (Horie et al., 2016).

We found the characteristic abnormal NF accumulation in a subset of $Dst^{Gt}$ homozygous Mo5 neurons, in cell bodies and spheroids (Fig. 1B). As previously shown in a chimera assay, NF accumulation in spinal cord neurons is due to a cell-autonomous effect of *Dst* deficiency (Campbell and Peterson, 1992). It is conceivable that *Dst* deficiency is the major cause of NF accumulation in the Mo5 motoneurons, taking into consideration that *Dst* is a cytoskeletal linker protein (Brown at el., 1995; Yang at el., 1996), and that it is highly expressed by neurons in the Mo5 nucleus (Horie et al., 2014). It is still unknown why NF accumulation occurs only in a subset of Mo5 motoneurons and not all Mo5 motoneurons. One possible reason is that NF filament accumulation occurs as a multistep event involving a cell-autonomous effect (*Dst* deficiency) and a non-cell-autonomous effect(s). We assume that axon damage is one of the additional factors, because there is massive macrophage infiltration into the V3 nerve, which may cause inflammation and axon damage (Martini and Willison, 2016). It is interesting to note that there is no NF accumulation in the cytoplasm of neurons in the hypoglossal nucleus (data not shown, Horie et al., 2014), probably because the hypoglossal nerve (XII) contains only axons of motoneurons, whereas the V3 nerve contains not only motor axons but also sensory axons, which also degenerate in *dt* mice (Sotelo and Guenet, 1988; Ichikawa et al., 2008). As for stress marker expression, cytoplasmic NF accumulation itself seems to stress neurons, because most neurons with cytoplasmic NF accumulation expressed stress markers (Fig. 1). It has been reported that *Lcn2* is a target gene of ER stress pathways (Hsin et al., 2012; El Karouli et al., 2015), and that neuron-derived Lcn2 serves as a “help-me” signal for glial cell activation (Xing et al., 2014).

Since previous studies have reported that NeuN-positive neurons were significantly decreased in the Mo5 nuclei of *dt* mice (De Repentigny et al., 2011; Horie et al., 2014), we tried to detect apoptosis using cleaved caspase 3 IHC (Fig. 4B; c). We successfully detected cleaved caspase 3 signals in Mo5 nuclei, and also co-localization of ChAT and cleaved

caspase 3 signals, indicating apoptosis of Mo5 motoneurons (Fig. 4B; d, insets). Interestingly, we also found some cleaved caspase 3 single positive cells, which were ChAT negative (Fig. 4B; d), indicating that other types of neurons in addition to motoneurons are also dying. Since some inhibitory interneurons were found within Mo5 nuclei (Li et al., 2005), they may undergo apoptosis in the $Dst^{Gt}$ homozygous Mo5 nuclei.

Finally, we examined the masseter muscle, the biting muscle innervated by Mo5 motoneurons, and found muscle atrophy (Fig. 6). We found muscle spindle degeneration in the $Dst^{Gt}$ homozygous masseter (Fig. 6), consistent with previous reports (Dowling et al., 1997; Duchen et al., 1963). In addition, we also found uncoordinated and weak masseter muscle contraction in $Dst^{Gt}$ homozygous mice (Fig. 7D). At present, we cannot distinguish whether the muscle atrophy is caused by cell-autonomous effects (*Dystonin-1b* deficiency) and/or non-cell-autonomous effects (e.g., Mo5 motoneuron degeneration or disuse). In order to answer this question, generation of *Dystonin-1b* specific knockout (KO) mice, or muscle-specific *Dst* conditional KO mice would be useful (Horie et al., 2017). Taken together, our data strongly suggests that masseter muscles of *dt* mutants have weak and uncoordinated movement; therefore, *dt* mice have difficulty in mastication.

**Acknowledgements**

This study was supported by research grants from the Ministry of Education, Culture, Sports, Science, and Technology of Japan (JP15H04667, JP16K15168, JP24700351), Grant-in-Aid for Scientific Research on Innovative Areas, “Glial assembly” (JP25117007), the Cooperative Study Program of National Institute for Physiological Sciences, and a Grant from the Niigata University Kyowakai Society (IH). We thank Dr. Atsushi Nambu, Dr. Hiromi Sano, Dr. Satomi Chiken, Dr. Kazuki Kuroda and Dr. Yoshihide Satoh for discussion, Dr. Li Zhou, Mr. Tomofumi Sakai, Dr. Yukiko Mori, Mr. Yuya Imada and Ms. Satoko

Yamagiwa for technical assistance, and all members of Takebayashi lab for suggestions and advice. The authors declare no conflict of interest.

**References**

Ariyasinghe S, Inoue M, Yamamura K, Harasawa Y, Kurose M, Yamada Y. 2004. Coordination of jaw and extrinsic tongue muscle activity during rhythmic jaw movements in anesthetized rabbits. Brain Res. 1016 (2), 201–216.

Baverstock, H., Jeffery, N.S., Cobb, S.N., 2013. The morphology of the mouse masticatory musculature. J Anat. 223 (1), 46–60.

Brown, A., Bernier, G., Mathieu, M., Rossant, J., Kothary, R., 1995. The mouse dystonia musculorum gene is a neural isoform of bullous pemphigoid antigen 1. Nat. Genet. 10 (3), 301–306.

Campbell, R.M., Peterson, A.C., 1992. An intrinsic neuronal defect operates in dystonia musculorum: a study of dt/dt<==>+/+ chimeras. Neuron 9 (4), 693–703.

Chien, M.H., Ying, T.H., Yang, S.F., Yu, J.K., Hsu, C.W., Hsieh, S.C., Hsieh, Y.H., 2012. Lipocalin-2 induces apoptosis in human hepatocellular carcinoma cells through activation of mitochondria pathways. Cell Biochem. Biophys. 64 (3), 177–186.

De Repentigny, Y., Ferrier, A., Ryan, S.D., Sato, T., Kothary, R., 2011. Motor unit abnormalities in *Dystonia musculorum* mice. PLoS One 6 (6), e21093.

Devireddy, L.R., Teodoro, J.G., Richard, F.A., Green, M.R., 2001. Induction of apoptosis by a secreted lipocalin that is transcriptionally regulated by IL-3 deprivation. Science 293 (5531), 829–834.

Dowling, J., Yang, Y., Wollmann, R., Reichardt, L.F., Fuchs, E., 1997. Developmental expression of BPAG1-n: Insights into the spastic ataxia and gross neurologic degeneration in *dystonia musculorum* mice. Dev. Biol. 187 (2), 131–142.

Duchen, L.W., Falconer, D.S., Strich, S.J., 1963. Dystonia musculorum: a hereditary neuropathy of mice affecting mainly sensory pathways. J. Physiol. 165, 7–9.

Duchen, L.W., Strich, S.J., Falconer, D.S., 1964. Clinical and pathological studies of a hereditary neuropathy in mice (dystonia musculorum). Brain 87, 367–378.

Edvardson, S., Cinnamon, Y., Jalas, C., Shaag, A., Maayan, C., Axelrod, F. B., Elpeleg, O., 2012. Hereditary sensory autonomic neuropathy caused by a mutation in dystonin. Ann. Neurol. 71 (4), 569–572.

El Karoui, K., Viau, A., Dellis, O., Bagattin, A., Nguyen, C., Baron, W., Burtin, M., Broueilh, M., Heidet, L., Mollet, G., Druilhe, A., Antignac, C., Knebelmann, B., Friedlander, G., Bienaimé, F., Gallazzini, M., Terzi, F., 2016. Endoplasmic reticulum stress drives proteinuria-induced kidney lesions via Lipocalin 2. Nat. Commun. 7, 10330.

Ferrier, A., Sato, T., De Repentigny, Y., Gibeault, S., Bhanot, K., O'Meara, R.W., Lynch-Godrei, A., Kornfeld, S.F., Young, K.G., Kothary, R., 2014. Transgenic expression of neuronal dystonin isoform 2 partially rescues the disease phenotype of the dystonia musculorum mouse model of hereditary sensory autonomic neuropathy VI. Hum. Mol. Genet. 23 (10), 2694–2710.

Furusho, M., Ono, K., Takebayashi, H., Masahira, N., Kagawa, T., Ikeda, K., Ikenaka, K., 2006. Involvement of the Olig2 transcription factor in cholinergic neuron development of the basal forebrain. Dev. Biol. 293 (2), 348–357.

Gomes, M.D., Lecker, S.H., Jagoe, R.T., Navon, A., Goldberg, A.L., 2001. Atrogin-1, a muscle-specific F-box protein, highly expressed during muscle atrophy. Proc. Natl. Acad. Sci. U S A 98 (25), 14440–14445.

Groves, R.W., Liu, L., Dopping-Hepenstal, P.J., Markus, H.S., Lovell, P.A., Ozoemena, L., Lai-Cheong, J.E., Gawler, J., Owaribe, K., Hashimoto, T., Mellerio, J.E., Mee, J.B., McGrath, J.A., 2010. A homozygous nonsense mutation within the dystonin gene coding for the coiled-coil domain of the epithelial isoform of BPAG1 underlies a new subtype of autosomal recessive epidermolysis bullosa simplex. J Invest Dermatol. 130 (6), 1551–1557.

Guo, L., Degenstein, L., Dowling, J., Yu, Q.C., Wollmann, R., Perman, B., Fuchs, E., 1995. Gene targeting of BPAG1: abnormalities in mechanical strength and cell migration in stratified epithelia and neurologic degeneration. Cell 81 (2), 233–243.

Hai, T., Wolfgang, C.D., Marsee, D.K., Allen, A.E., Sivaprasad, U., 1999. ATF3 and stress responses. Gene Expr. 7(4–6), 321–335

Halabian, R., Tehrani, H.A., Jahanian-Najafabadi, A., Habibi Roudkenar, M., 2013. Lipocalin-2-mediated upregulation of various antioxidants and growth factors protects bone marrow-derived mesenchymal stem cells against unfavorable microenvironments. Cell Stress Chaperones 18 (6), 785–800.

Horie, M., Meguro, R., Hoshino, K., Ishida, N., Norita, M., 2013. Neuroanatomical study on the tecto-suprageniculate-dorsal auditory cortex pathway in the rat. Neuroscience 228, 382–394.

Horie, M., Watanabe, K., Bepari, A.K., Nashimoto, J., Araki, K., Sano, H., Chiken, S., Nambu, A., Ono, K., Ikenaka, K., Kakita, A., Yamamura, K., Takebayashi, H., 2014.

Disruption of actin-binding domain-containing Dystonin protein causes *dystonia musculorum* in mice. Eur. J. Neurosci. 40 (10), 3458–3471.

Horie, M., Mekada, K., Sano, H., Kikkawa, Y., Chiken, S., Someya, T., Saito, K., Hossain, M.I., Nameta, M., Abe, K., Sakimura, K., Ono, K., Nambu, A., Yoshiki, A., Takebayashi, H., 2016. Characterization of novel dystonia musculorum mutant mice: implications for central nervous system abnormality. Neurobiol. Dis. 96, 271–283.

Horie M, Yoshioka N, Takebayashi H., 2017. BPAG1 in muscles: Structure and function in skeletal, cardiac and smooth muscle. Semin. Cell Dev. Biol. 69, 26–33.

Hsin, I.L., Hsiao, Y.C., Wu, M.F., Jan, M.S., Tang, S.C., Lin, Y.W., Hsu, C.P., Ko, J.L., 2012. Lipocalin 2, a new GADD153 target gene, as an apoptosis inducer of endoplasmic reticulum stress in lung cancer cells. Toxicol Appl Pharmacol. 263(3), 330–337.

Ichikawa, H., Terayama, R., Yamaai, T., De Repentigny, Y., Kothary, R., Sugimoto, T., 2008. The number of nociceptors in the trigeminal ganglion but not proprioceptors in the mesencephalic trigeminal tract nucleus is reduced in dystonin deficient dystonia musculorum mice. Brain Res. 1226, 33–38.

Ikeda, M., Hossain, M.I., Zhou, L., Horie, M., Ikenaka, K., Horii, A., Takebayashi, H. 2017. Histological detection of dynamic glial responses in the dysmyelinating *Tabby-jimpy* mutant brain. Anat. Sci. Int. *in press*

Janota, I., 1972. Ultrastructural studies of an hereditary sensory neuropathy in mice (dystonia musculorum). Brain 95 (3), 529–536.

Jha, M.K., Lee, S., Park, D.H., Kook, H., Park, K.G., Lee, I.K., Suk, K. 2015. Diverse functional roles of lipocalin-2 in the central nervous system. Neurosci. Biobehav. Rev. 49, 135–156.

Lee, S., Lee, J., Kim, S., Park, J.Y., Lee, W.H., Mori, K., Kim, S.H., Kim, I.K., Suk, K., 2007. A dual role of lipocalin 2 in the apoptosis and deramification of activated microglia. J. Immunol. 179 (5), 3231–3241.

Leung, C.L., Sun, D., Liem, R.K., 1999. The intermediate filament protein peripherin is the specific interaction partner of mouse BPAG1-n (dystonin) in neurons. J. Cell Biol. 144 (3), 435–446.

Leung, C.L., Zheng, M., Prater, S.M., Liem, R.K., 2001. The BPAG1 locus: alternative splicing produces multiple isoforms with distinct cytoskeletal linker domains, including predominant isoforms in neurons and muscles. J. Cell Biol. 154 (4), 691–697.

Li, Y.Q., Takada, M., Kaneko, T., Mizuno, N. 1995. Premotor neurons for trigeminal motor nucleus neurons innervating the jaw-closing and jaw-opening muscles: differential distribution in the lower brainstem of the rat. J. Comp. Neurol. 356 (4), 563–579.

Li, J.L., Wu, S.X., Tomioka, R., Okamoto, K., Nakamura, K., Kaneko, T., Mizuno, N., 2005. Efferent and afferent connections of GABAergic neurons in the supratrigeminal and the intertrigeminal regions. An immunohistochemical tract-tracing study in the GAD67-GFP knock-in mouse. Neurosci. Res. 51 (1), 81–91.

Liu, Z., Yang, A., Wang, Z., Bunting, K.D., Davuluri, G., Green, M.R., Devireddy, L.R., 2011. Multiple apoptotic defects in hematopoietic cells from mice lacking lipocalin 24p3. J. Biol. Chem. 286 (23), 20606–20614.

Manganelli, F., Parisi, S., Nolano, M., Tao, F., Paladino, S., Pisciotta, C., Tozza, S., Nesti, C., Rebelo, A.P., Provitera, V., Santorelli, F.M., Shy, M.E., Russo, T., Zuchner, S., Santoro, L., 2017. Novel mutations in *dystonin* provide clues to the pathomechanisms of HSAN-VI. Neurology 88 (22), 2132–2140.

Martini, R., Willison, H., 2016. Neuroinflammation in the peripheral nerve: Cause, modulator, or bystander in peripheral neuropathies? Glia 64 (4), 475–486.

N'gom, P.I., Woda, A., 2002. Influence of impaired mastication on nutrition. J. Prosthet. Dent. 87 (6), 667–673.

Nilsen-Hamilton, M., Liu, Q., Ryon, J., Bendickson, L., Lepont, P., Chang, Q., 2003. Tissue involution and the acute phase response. Ann. N. Y. Acad. Sci. 995, 94–108.

Okumura, M., Yamakawa, H., Ohara, O., Owaribe, K., 2002. Novel alternative splicings of BPAG1 (bullous pemphigoid antigen 1) including the domain structure closely related to MACF (microtubule actin cross-linking factor). J. Biol. Chem. 277 (8), 6682–6687.

Ootaki, S., Yamamura, K., Inoue, M., Amarasena, J.K., Kurose, M., Yamada, Y., 2004. Activity of peri-oral facial muscles and its coordination with jaw muscles during ingestive behavior in awake rabbits. Brain Res. 1001 (1-2), 22-36.

Ryan, S.D., Ferrier, A., Kothary, R., 2012a. A novel role for the cytoskeletal linker protein dystonin in the maintenance of microtubule stability and the regulation of ER-Golgi transport. BioArchitecture 2 (1), 2–5.

Ryan, S.D., Bhanot, K., Ferrier, A., De Repentigny, Y., Chu, A., Blais, A., Kothary, R., 2012b. Microtubule stability, Golgi organization, and transport flux require dystonin-a2-MAP1B interaction. J. Cell Biol. 196 (6), 727–742.

Sandri, M., Sandri, C., Gilbert, A., Skurk, C., Calabria, E., Picard, A., Walsh, K., Schiaffino, S., Lecker, S.H., Goldberg, A.L., 2004. Foxo transcription factors induce the atrophy-related ubiquitin ligase atrogin-1 and cause skeletal muscle atrophy. Cell 117 (3), 399–412.

Seehusen, F., Kiel, K., Jottini, S., Wohlsein, P., Habierski, A., Seibel, K., Vogel, T., Urlaub, H., Kollmar, M., Baumgärtner, W., Teichmann, U., 2016. Axonopathy in the central nervous system is the hallmark of mice with a novel Intragenic null mutation of Dystonin. Genetics 204 (1), 191–203.

Sotelo, C., Guenet, J.L., 1988. Pathologic changes in the CNS of dystonia musculorum mutant mouse: an animal model for human spinocerebellar ataxia. Neuroscience 27 (2), 403–424.

Takebayashi, H., Nabeshima, Y., Yoshida, S., Chisaka, O., Ikenaka, K., Nabeshima, Y., 2002. The basic helix-loop-helix factor olig2 is essential for the development of motoneuron and oligodendrocyte lineages. Curr. Biol. 12 (13), 1157–1163.

Tong, Z., Wu, X., Kehrer, J.P., 2003. Increased expression of the lipocalin 24p3 as an apoptotic mechanism for MK886. Biochem. J. 372 (Pt 1), 203–210.

Tong, Z., Wu, X., Ovcharenko, D., Zhu, J., Chen, C.S., Kehrer, J.P., 2005. Neutrophil gelatinase-associated lipocalin as a survival factor. Biochem. J. 391 (Pt 2), 441–448.

Tseng, K.W., Chau, Y.P., Yang, M.F., Lu, K.S., Chien, C.L., 2008. Abnormal cellular translocation of α-internexin in spinal motor neurons of *Dystonia musculorum* mice. J. Comp. Neurol. 507 (1), 1053–1064.

Watanabe, K., Tamamaki, N., Furuta, T., Ackerman, S.L., Ikenaka, K., Ono, K., 2006. Dorsally derived netrin 1 provides an inhibitory cue and elaborates the 'waiting period' for primary sensory axons in the developing spinal cord. Development 133 (7), 1379–1387.

Westgate, G.E., Weaver, A.C., Couchman, J.R., 1985. Bullous pemphigoid antigen localization suggests an intracellular association with hemidesmosomes. J. Invest. Dermatol. 84 (3), 218–224.

Wolfgang, C.D., Chen, B.P., Martindale, J.L., Holbrook, N.J., Hai, T., 1997. gadd153/Chop10, a potential target gene of the transcriptional repressor ATF3. Mol. Cell Biol. 17(11): 6700–6707.

Xing, C., Wang, X., Cheng, C., Montaner, J., Mandeville, E., Leung, W., van Leyen, K., Lok, J., Wang, X., Lo, E.H., 2014. Neuronal production of lipocalin-2 as a help-me signal for glial activation. Stroke 45 (7), 2085–2092.

Yang, Y., Dowling, J., Yu, Q.C., Kouklis, P., Cleveland, D.W., Fuchs, E., 1996. An essential cytoskeletal linker protein connecting actin microfilaments to intermediate filaments. Cell 86 (6), 655–665.

Young, K.G., Kothary, R., 2007. Dystonin/Bpag1- A link to what? Cell Motil. Cytoskeleton 64 (12), 897–905.

**Figure legends**

**Fig. 1. Histological abnormalities of Mo5 neurons in the brainstem of *Dst*$^{Gt}$ homozygote at P28. A**) Representative image of the Mo5 nucleus in the brainstem. The dot lined circle shows Mo5 nucleus, which is shown in high magnification in B and C. **B**) Coronal brainstem sections were stained with NF IHC, *CHOP* ISH and *ATF3* ISH of wild-type (WT) and *Dst*$^{Gt}$ homozygous (*Dst*$^{Gt}$ homo) brain, which were counterstained with hematoxylin for IHC and nuclear fast red for ISH. Arrowheads indicate positive cells. **C**) Co-localization of abnormal NF-accumulation signal with *CHOP* signal (red arrowhead; g, g') and *ATF3* signal (red arrowhead; h, h') in Mo5 nucleus of *Dst*$^{Gt}$ homozygotes (*Dst*$^{Gt}$ homo). Co-localization of ATF3 signal and *CHOP* signal (i, i') in the Mo5 neuron of *Dst*$^{Gt}$ homozygous mice. Red arrowheads indicate double positive cells while black arrowheads indicate ATF3-single positive nucleus. Red rectangle in g, h and i was shown in g', h' and i', respectively. Note that ATF3 signals are observed in the nuclei of cells. **D-F)** Statistical analyses (Mann-Whitney U test) of abnormal NF accumulation (D), *CHOP*-positive cells (E) and *ATF3*-positive cells (F) in the Mo5 nuclei (*$P$ < 0.05, **$P$ < 0.01). Scale bars: 1 mm (A), 100 μm (g, h, and i of C), 50 μm (a-f of B) and 20 μm (g' h', and i' of C).

**Fig. 2. Lcn2 expression in the Mo5 motoneurons of *Dst*$^{Gt}$ homozygous mice. A**) Coronal sections were stained with *Lcn2* ISH (a, b) and Lcn2 IHC (c, d) of wild-type (WT; a, c) and *Dst*$^{Gt}$ homozygous (*Dst*$^{Gt}$ homo; b, d) brain at P28. Arrowheads indicate positive signals in each case. **B**) Statistical significance of *Lcn2* expression in the Mo5 motoneurons at P21 and P28 was evaluated by Mann-Whitney U test (*$P$ < 0.05). **C**) Cholera toxin B subunit (CTB) was injected into the masseter muscle of both wild-type (WT) and *Dst*$^{Gt}$ homozygous (*Dst*$^{Gt}$ homo) mice at P18. Three days later, mice were sacrificed, and then, coronal sections were stained with anti-CTB IHC (e, f) and double stained with *Lcn2* ISH and CTB IHC (g, h).

Arrowheads indicate double positive cells for Lcn2 signal and CTB signal in the Mo5 motoneurons of *Dst*$^{Gt}$ homozygous mice. Scale bars: 50 μm.

**Fig. 3. Reduction of the number of Mo5 motoneurons and the size of Mo5 nucleus in the *Dst*$^{Gt}$ homozygous mice at P28. A**) Coronal sections were stained with choline acetyltransferase (ChAT) IHC for wild-type (WT) and *Dst*$^{Gt}$ homozygous (*Dst*$^{Gt}$ homo) brain at P28. Black rectangles in a and b were shown in a' and b', respectively. **B**) Statistical analysis of ChAT-positive Mo5 motoneurons of wild-type (WT) and *Dst*$^{Gt}$ homozygous (*Dst*$^{Gt}$ homo) brain at P28. Statistical significance was evaluated by *t*-test (**P* < 0.05). **C**) Statistical analysis of the size of Mo5 nucleus through AP axis of wild-type (WT) and *Dst*$^{Gt}$ homozygous (*Dst*$^{Gt}$ homo) brain at P28. Statistical significance was evaluated by *t*-test (***P* < 0.01). Scale bars: 1 mm (a and b of A), 100 μm (a' and b' of A).

**Fig. 4. Induction of apoptotic marker in the Mo5 nucleus of *Dst*$^{Gt}$ homozygote mice at P28. A**) Representative image of brainstem to show the Mo5 nucleus. The dotted circle shows Mo5 nucleus and this part of brainstem, which is shown in high magnification in B. **B**) Coronal sections were stained with cleaved caspase 3 IHC (a, b) and double staining with ChAT ISH and cleaved caspase 3 IHC (c, d) for wild-type (WT) and *Dst*$^{Gt}$ homozygous (*Dst*$^{Gt}$ homo) brain at P28. Arrowheads indicate cleaved caspase 3-positive cells. Small red rectangles in d were shown in insets as indicated. **C**) Statistical analysis of cleaved caspase 3-positive Mo5 motoneurons of wild-type (WT) and *Dst*$^{Gt}$ homozygous (*Dst*$^{Gt}$ homo) brain at P28. Statistical significance was evaluated by Mann-Whitney U test (**P* < 0.05). **D**) Double fluorescent IHC of NF (green, e), cleaved caspase 3 (red, f) counterstained with DAPI (blue, g) for *Dst*$^{Gt}$ homozygous (*Dst*$^{Gt}$ homo) brain at P28. Merged image was shown in h. Red arrowhead indicates the same cell. Scale bars: 1 mm (A), 50 μm (a-d of B) and 50 μm (e-h of

D).

**Fig. 5. Macrophage infiltration in the V3 branch of trigeminal nerve of *Dst*$^{Gt}$ homozygote mice at P28. A**) HE staining of V3 nerve (a, b) of wild-type (WT) and *Dst*$^{Gt}$ homozygote (*Dst*$^{Gt}$ homo) at P28. Note that, there are more nuclei in the V3 nerve of *Dst*$^{Gt}$ homozygous mice than that of wild-type mice. **B**) Increaded number of nuclei was observed in the V3 nerve of *Dst*$^{Gt}$ homozygotes (*t*-test, $^{**}P < 0.01$). **C**) GFAP IHC (c, d) and Iba1 IHC (e, f) of V3 nerve of wild-type (WT) and *Dst*$^{Gt}$ homozygous (*Dst*$^{Gt}$ homo) at P28. Note that Iba1-positive macrophages are increased in the V3 nerve of *Dst*$^{Gt}$ homozygotes. **D**) Double IHC of MBP (g, h) and Iba1 (i, j) in the V3 nerve of wild-type (WT) and *Dst*$^{Gt}$ homozygous (*Dst*$^{Gt}$ homo) at P28. Merged image was shown in k, l. Note that MBP-positive axons are co-localized with Iba1-positive macrophages in the V3 nerve of *Dst*$^{Gt}$ homozygous. Scale bars: 20 μm.

**Fig. 6. Atrophy of masseter muscle of *Dst*$^{Gt}$ homozygous mice at P28. A**) Gross image of masseter muscles of wild-type (WT) and *Dst*$^{Gt}$ homozygous (*Dst*$^{Gt}$ homo) at P28. Note that, masseter muscles of *Dst*$^{Gt}$ homozygous mice are smaller and thinner than those of wild-type mice. **B**) HE staining of masseter muscle of wild-type (a) and *Dst*$^{Gt}$ homozygous (b) mice at P28. Some of myofibrils of *Dst*$^{Gt}$ homozygous mice show dense nuclei than those of wild-type mice. **C**) *Atrogin-1* ISH of masseter muscles of wild-type (WT) and *Dst*$^{Gt}$ homozygous (*Dst*$^{Gt}$ homo) at P28. Both longitudinal (c, d) and cross sections (e, f) of masseter muscle showed increased *atrogin-1* expression. Black rectangles are shown at high magnifications in insets in each case. **D**) HE staining of the cross sections of myofibrils shows muscle spindles of *Dst*$^{Gt}$ homozygous mice masseter are abnormal, either swollen (i) or degenerating (j) when compared with fine shaped and well-defined (g, h) muscle spindles of wild-type mice

masseter. MYH6 IHC also shows abnormal muscle spindle either swollen (m) or degenerating (n) structure in the *Dst*$^{Gt}$ homozygous mice masseter. Scale bars: 200 μm (c and d of C), 100 μm (e and f of C), 50 μm (a and b of B; insets of c, d) and 20 μm (g-n of D; insets of e, f).

**Fig. 7. EMG recording in the masseter muscle and the suprahyoid muscle of *Dst*$^{Gt}$ homozygous mice and control mice at P28. A**) Graphs showing representative EMG data at resting state (four *Dst*$^{Gt}$ homozygous mice at P24 and three control mice at P24). EMG data showed that the *Dst*$^{Gt}$ homozygous mouse (P24) showed overlap of masseter (closing) and suprahyoid (opening) muscle activities, whereas no such contraction was observed in the control mouse (P24). **B**) Graphs showing representative EMG data at active state. **C**) Duration of masseter at active state tends to become longer with no statistically significance. **D**) AUC of masseter activity showed significantly lower response in *Dst*$^{Gt}$ homozygous mouse. Statistical significance was evaluated by *t*-test (*$P < 0.05$).

**sFig. 1. Reduced size of Mo5 nucleus of *Dst*$^{Gt}$ homozygous mice at P28.** Coronal sections were stained with motoneuron marker ChAT IHC to stain the Mo5 motoneurons for wild-type (WT) and *Dst*$^{Gt}$ homozygous (*Dst*$^{Gt}$ homo) brain at P28. Black rectangle was shown at high magnification in adjacent place in each case. Scale bars: 1 mm (a-r) and 100 μm (a'-r').

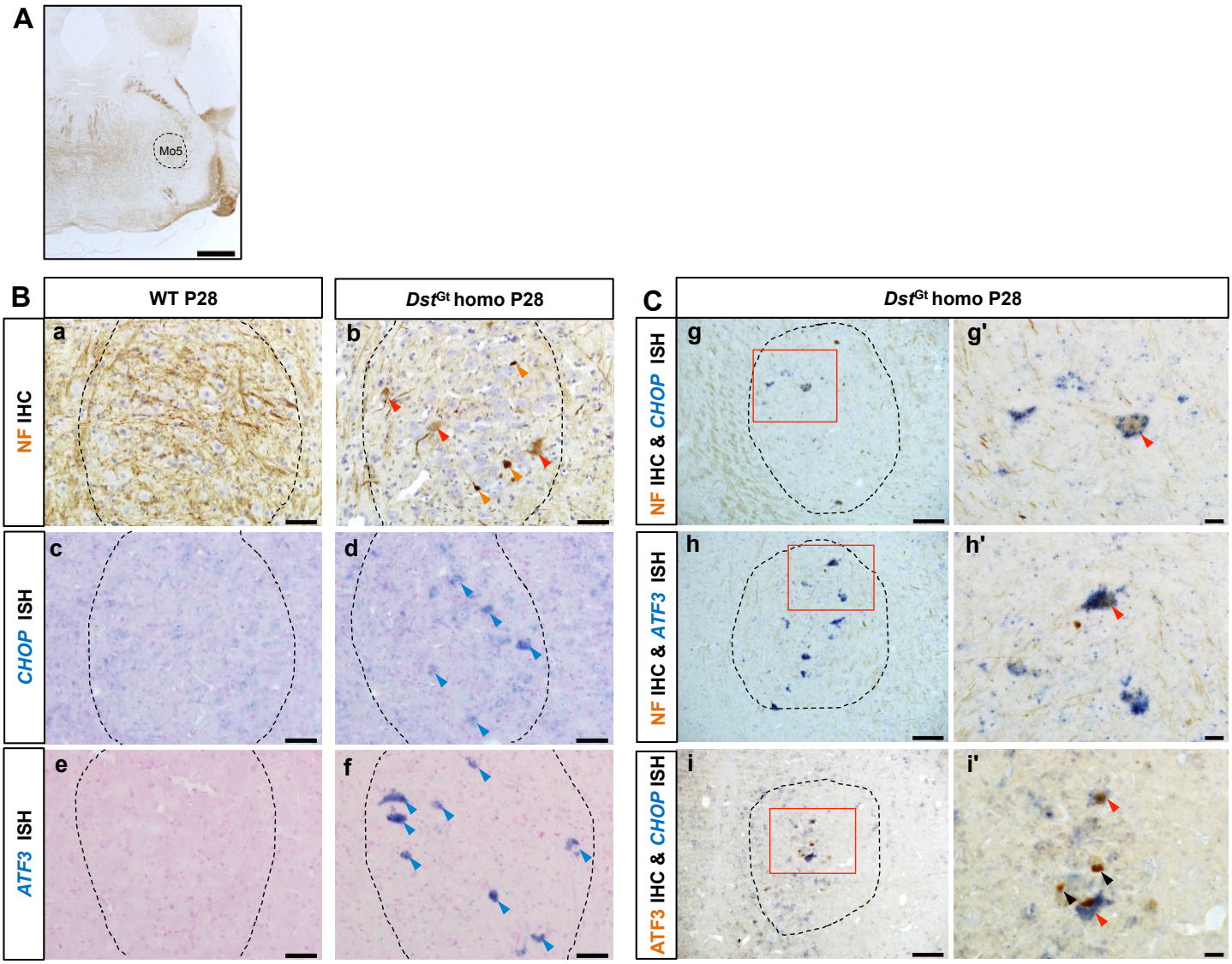


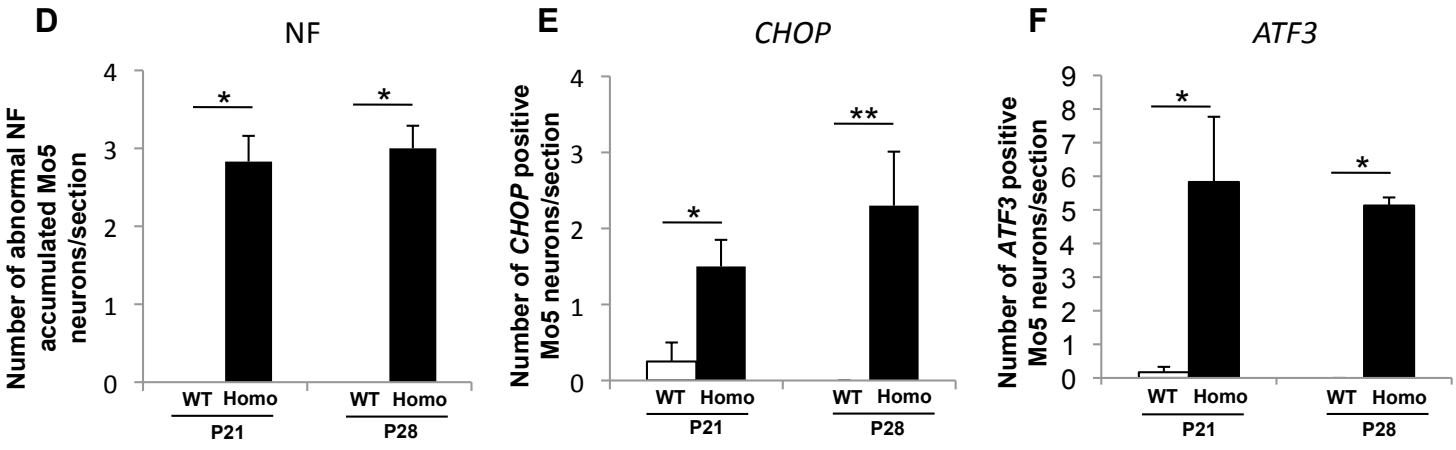


Hossain et *al.* Figure 1

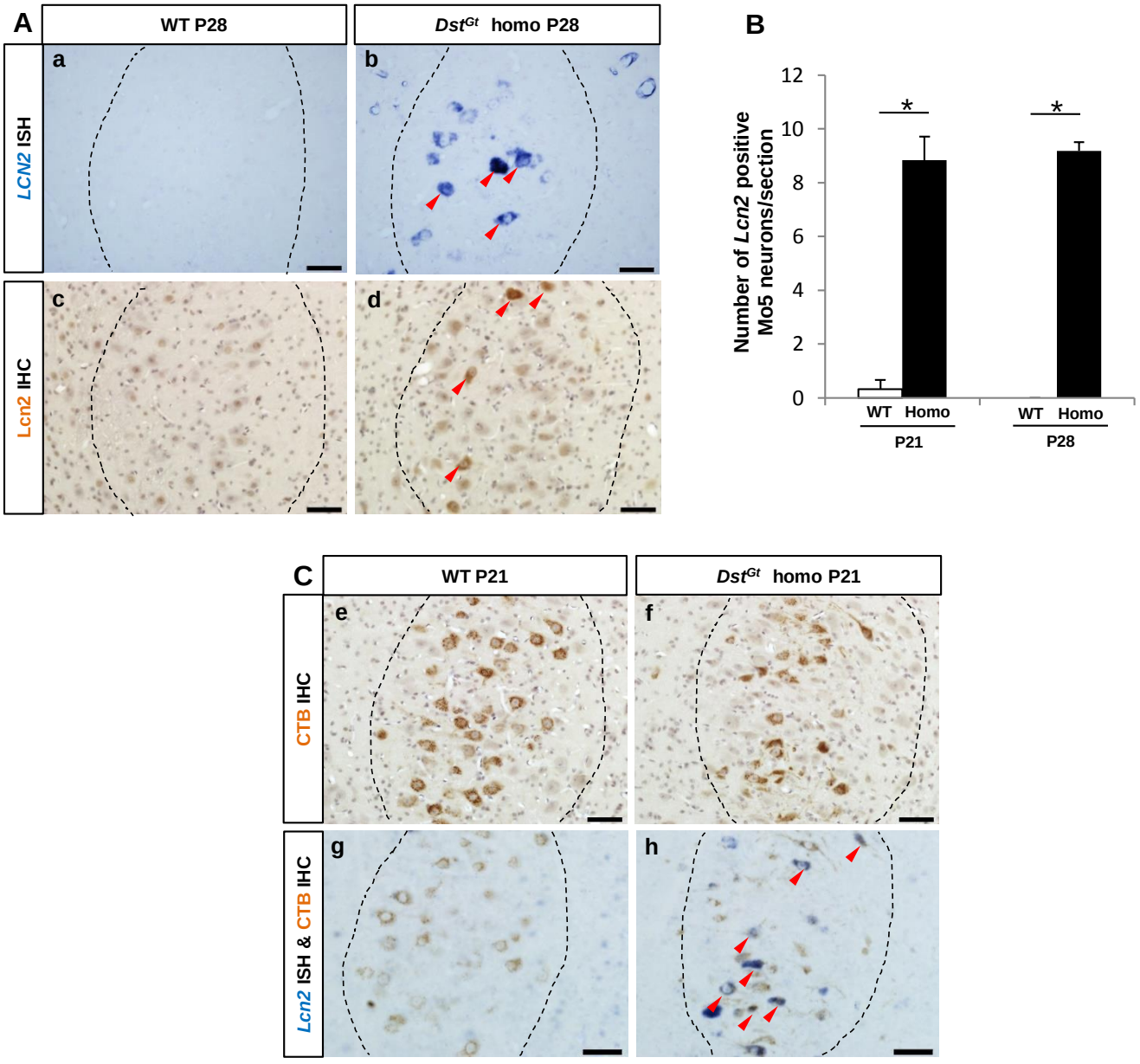


**Hossain *et al*. Figure 2**

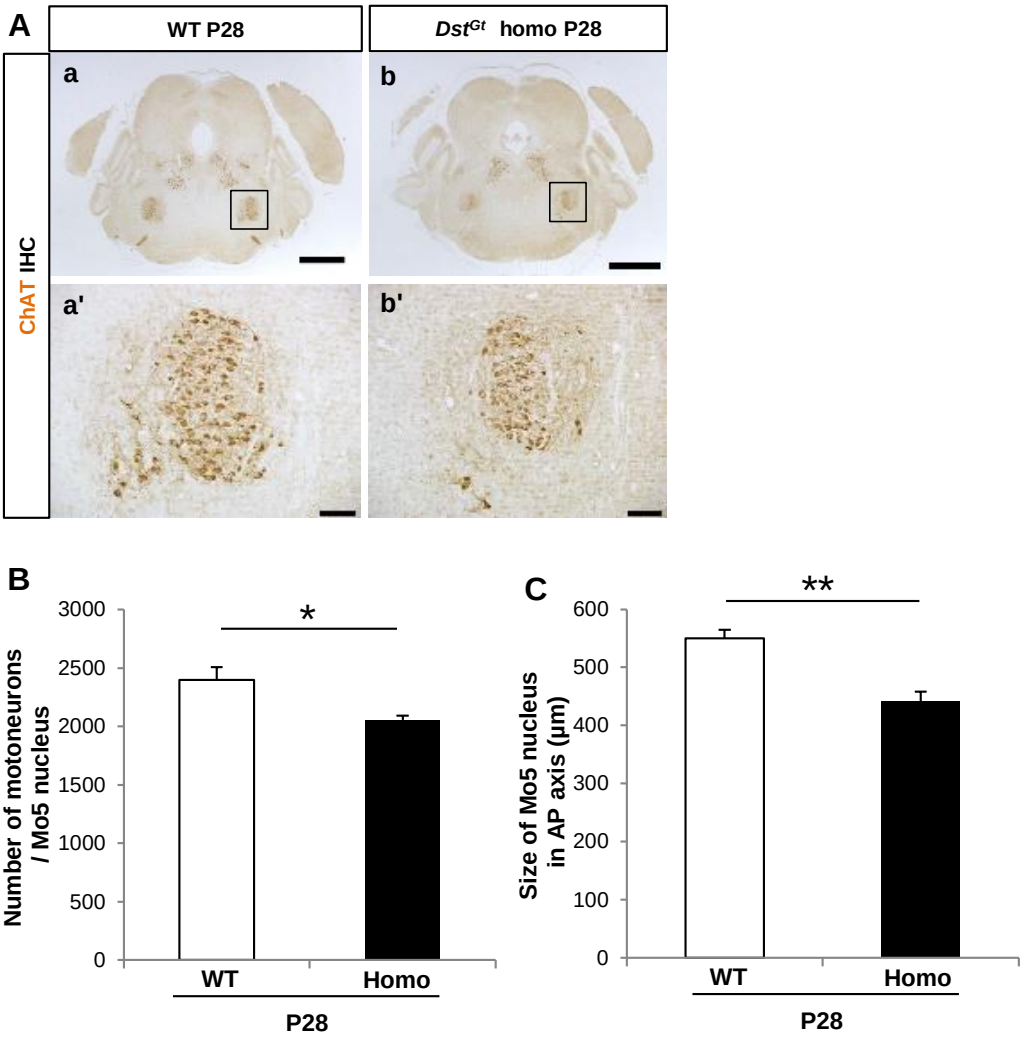


**Hossain et *al*. Figure 3**

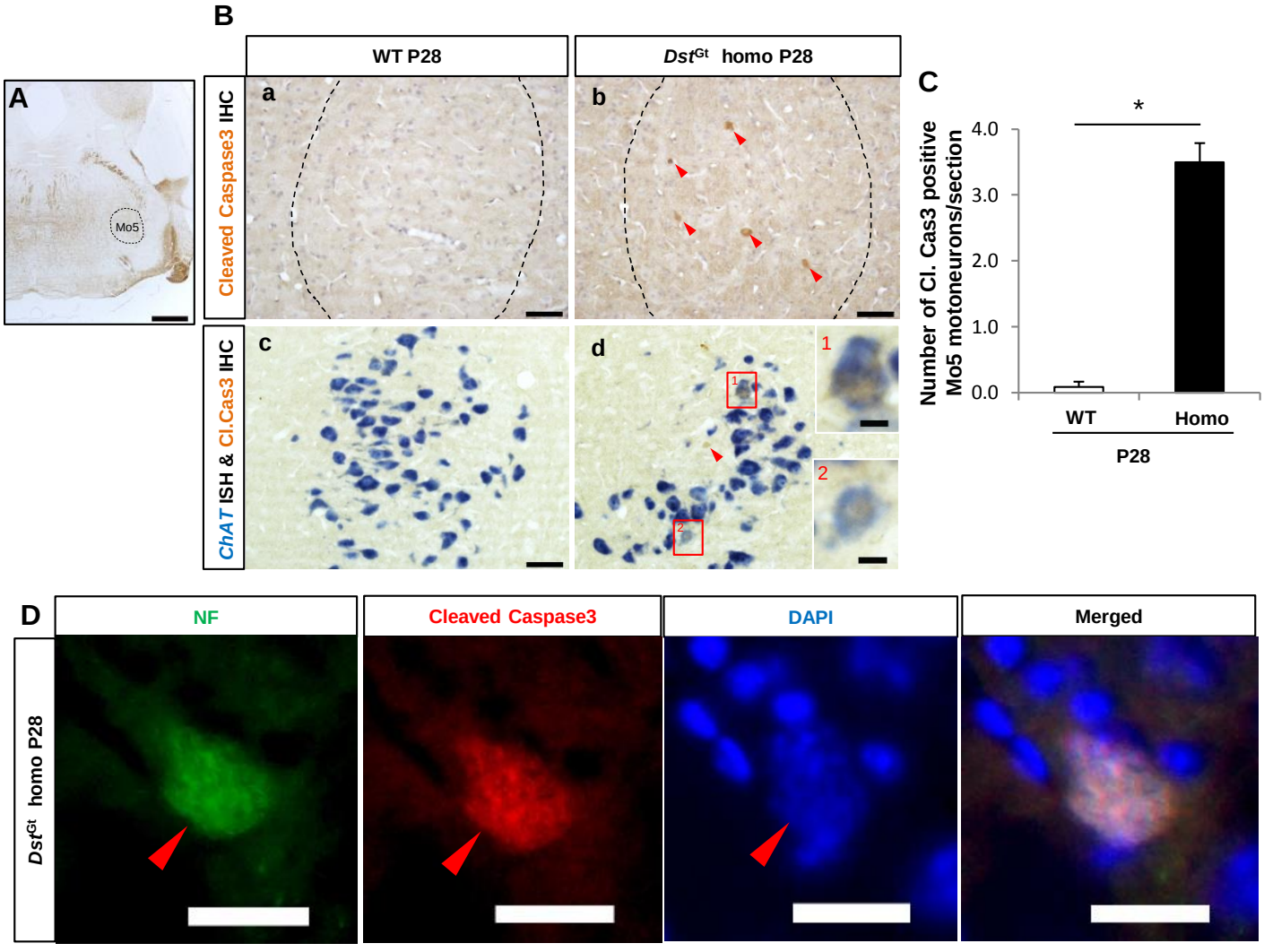


Hossain *et al*. Figure 4

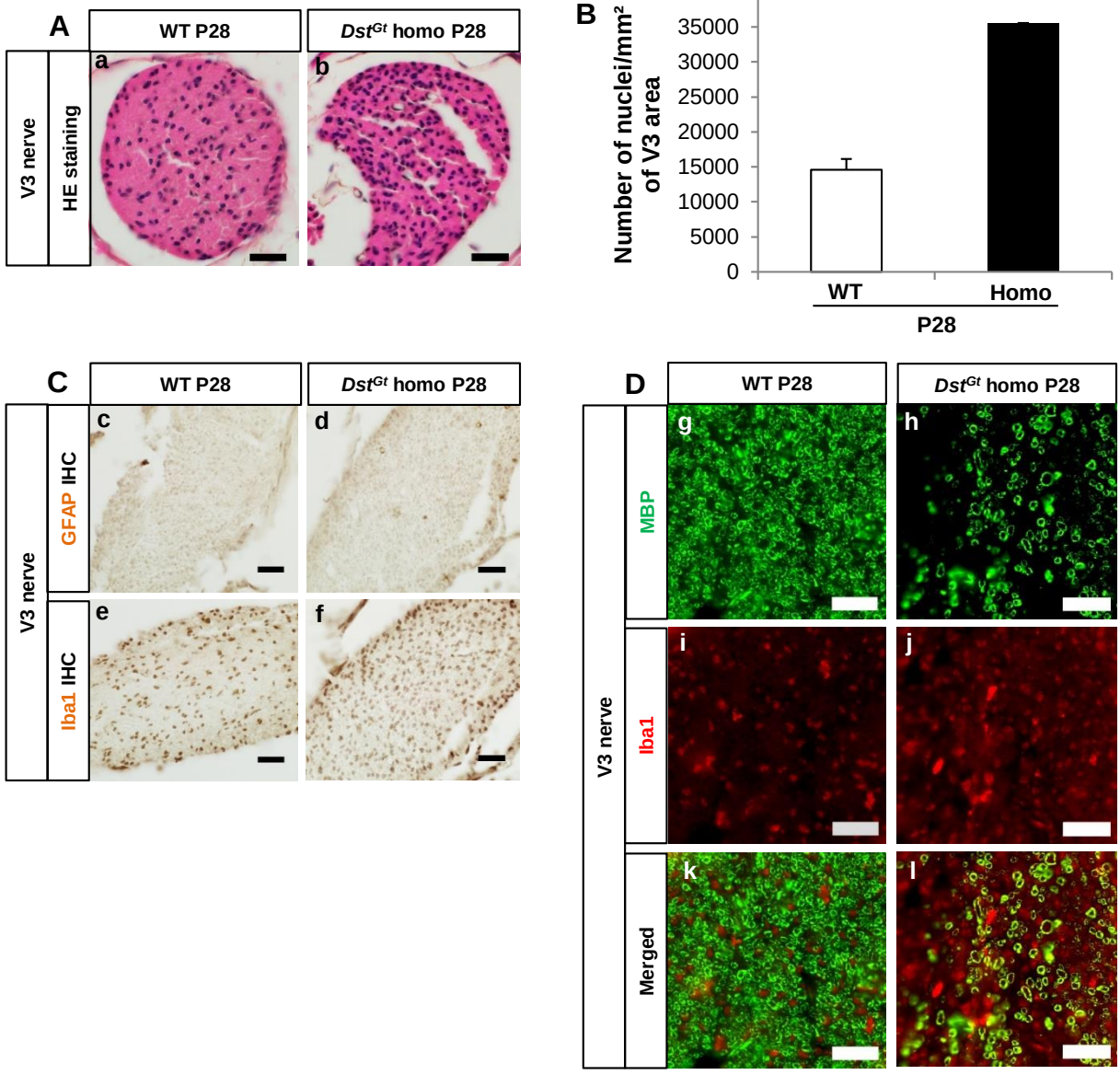


**Hossain e*t al*. Figure 5**

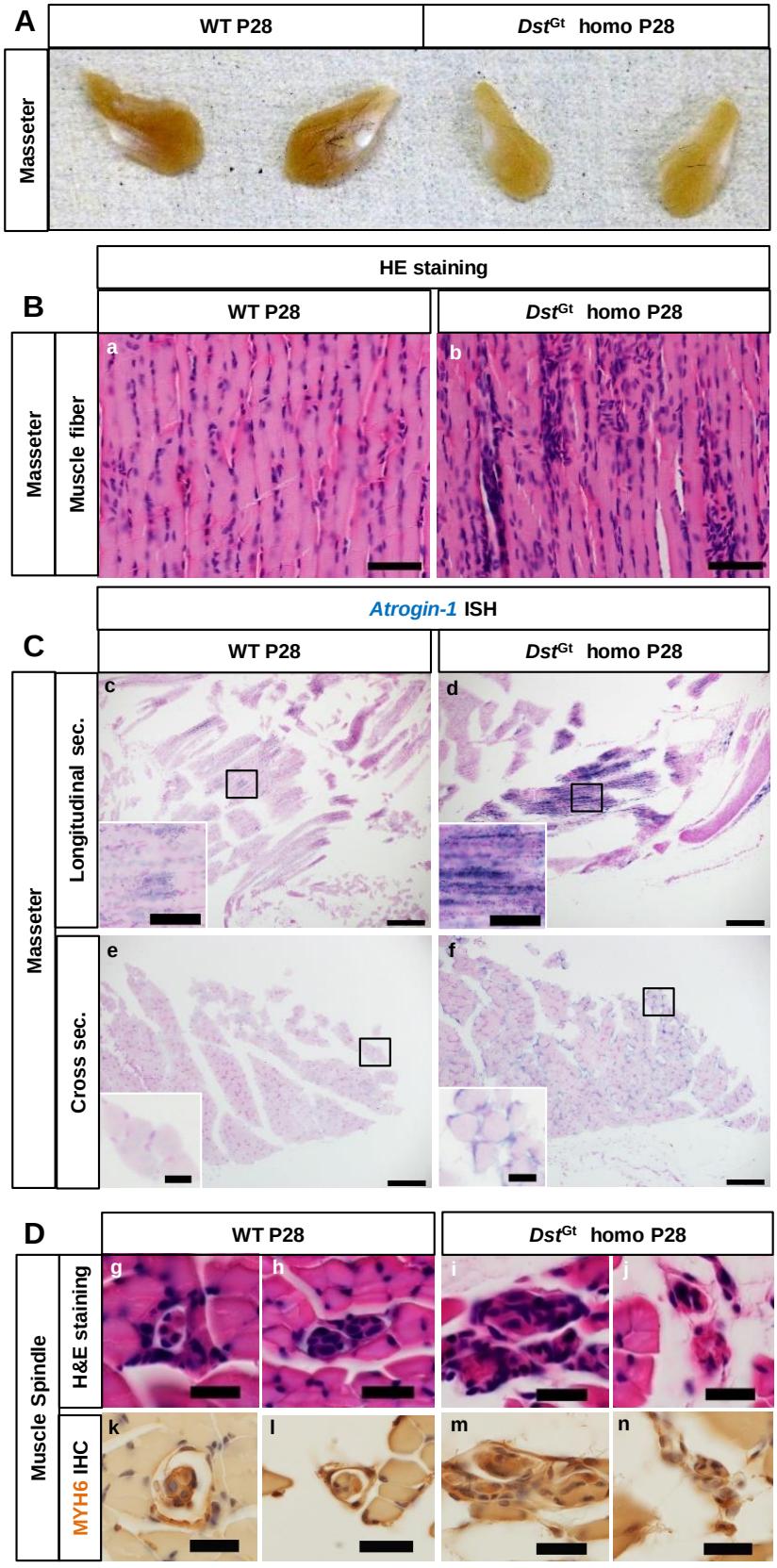


Hossain *et al*. Figure 6

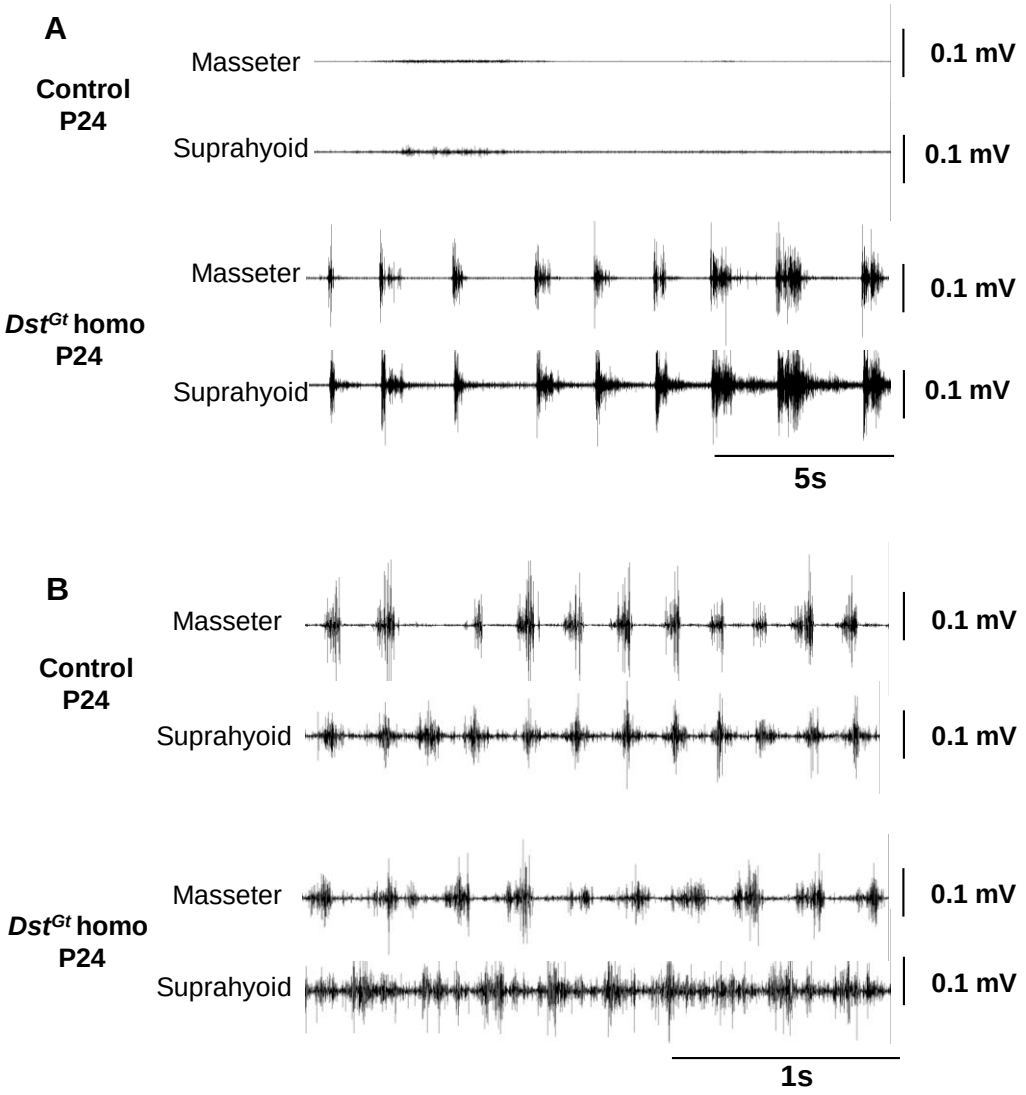


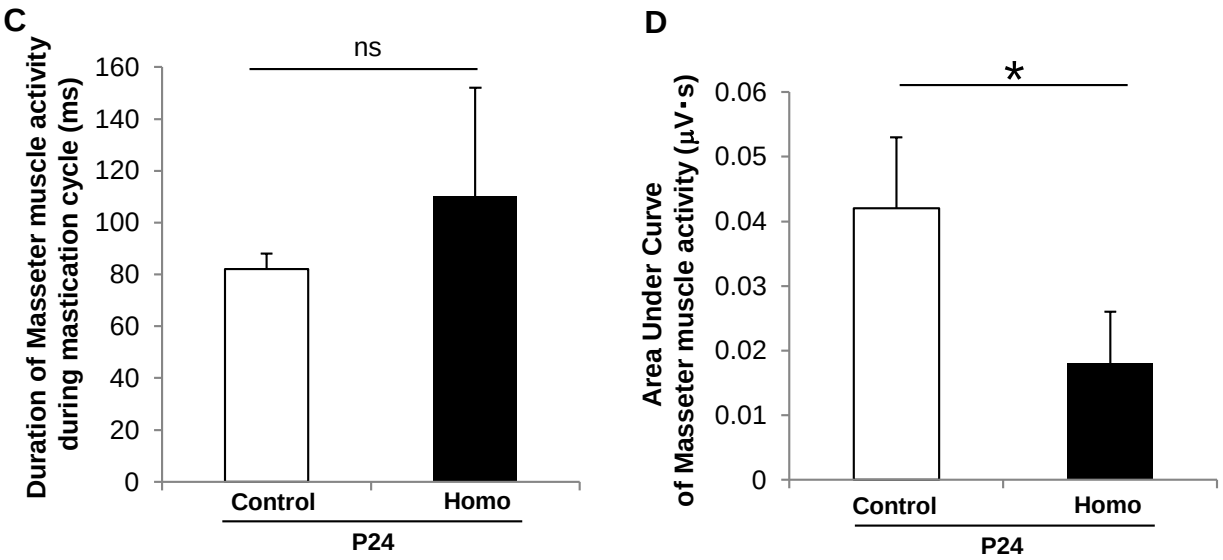


**Hossain *et al*. Figure 7**

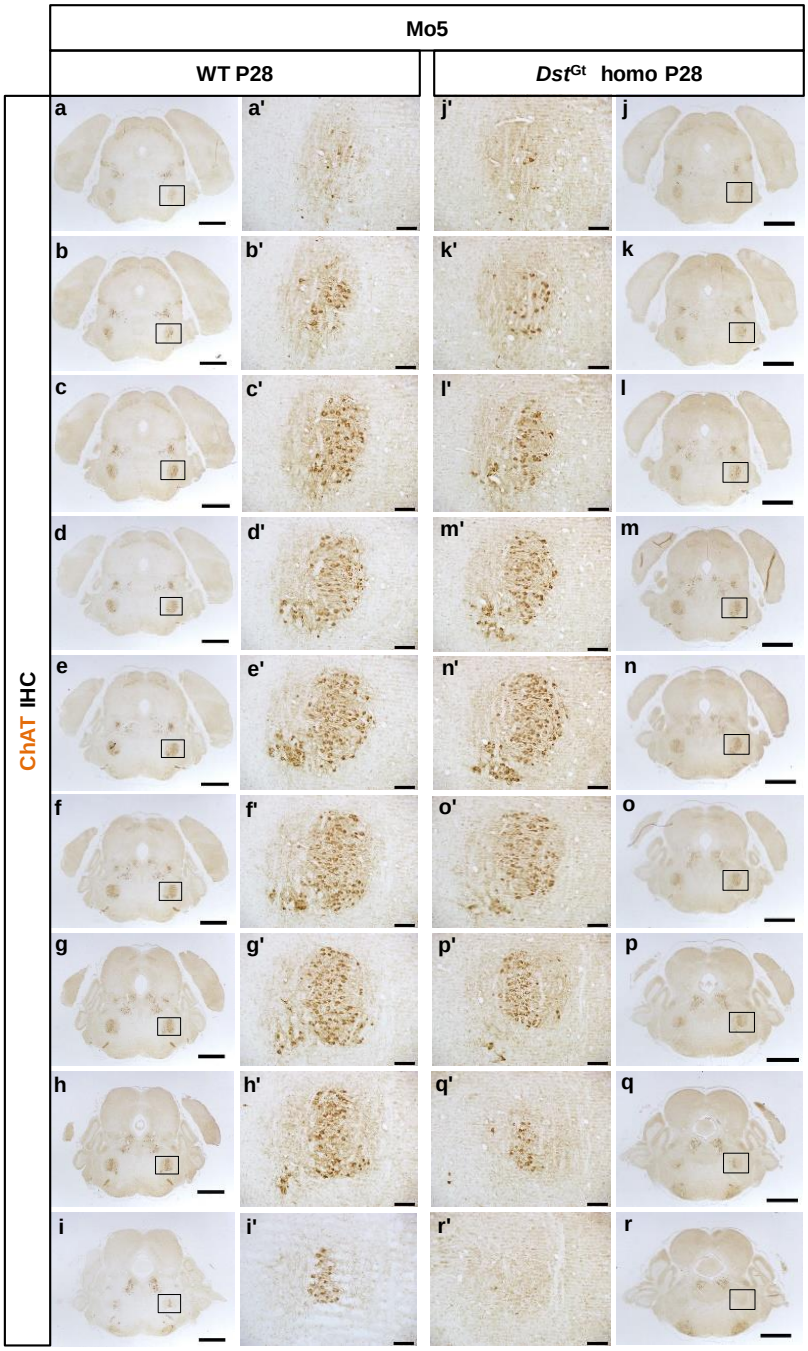


**Hossain e*t al*. Figure s1**